Microporous and Mesoporous Materials 116 (2008) 633–640

Contents lists available at ScienceDirect

Microporous and Mesoporous Materials

journal homepage: www.elsevier.com/locate/micromeso

Homopolymer induced phase evolution in mesoporous silica from evaporation induced self-assembly process

Chong Liu [a], Yonghui Deng [a,*], Jia Liu [a], Haihong Wu [b], Dongyuan Zhao [a,*]

[a] Department of Chemistry, Shanghai Key Laboratory of Molecular Catalysis and Innovative Materials, Advanced Materials Laboratory, Fudan University, Shanghai 200433, PR China
[b] Shanghai Key Laboratory of Green Chemistry and Chemical Processes, Department of Chemistry, East China Normal University, Shanghai 200062, PR China

ARTICLE INFO

Article history:
Received 14 April 2008
Received in revised form 18 May 2008
Accepted 26 May 2008
Available online 5 June 2008

Keywords:
Mesoporous materials
Homopolymer
Triblock copolymer
Synthesis
Templating

ABSTRACT

In this paper, we report the experimental findings on the phase evolution of mesoporous silica in an evaporation induced self-assembly (EISA) approach by using low molecular weight homopolymer poly(propylene oxide) (M_n = 400, PPO400) as an additive. It is found that the addition of PPO400 can cause hydrotropic curvature-reducing effect on the mesostructures. Upon the increase of PPO400 addition amount, the structures of the obtained mesoporous silicas gradually evolve from three-dimensional (3-D) cubic $Im\bar{3}m$ to quasi-*p6m*, to hexagonal *p6m*, and to mixed structures consisting of lamellar and reversed cylindrical structure. The quasi-*p6m* mesoporous silica structure has the buckled cylindrical mesopores with intermediate curvature and acts as the metastable structure during the phase evolution from $Im\bar{3}m$ to *p6m* structure. We ascribe this curvature-reducing effect to the relatively weak hydrophobicity and good compatibility of PPO400 homopolymer. Moreover, the condition with larger homopolymer PPO4000 (M_n = 4000) as the additive has been also investigated and discussed.

1. Introduction

Ordered mesoporous materials have received much attention because of their widespread applications [1–6]. As one of the momentous breakthroughs in ordered mesoporous materials, the templating synthesis based on nonionic surfactants as the structure directing agents (SDAs) has brought out various highly ordered mesoporous materials [7–15]. In particular, by using triblock copolymers poly(ethylene oxide)-*b*-poly(propylene oxide)-*b*-poly(ethylene oxide) (PEO-PPO-PEO) as templates and through various strategies, a large number of ordered mesoporous materials with different structures, have been successfully synthesized [7,8]. This structure abundance endows the mesoporous materials with diverse properties which could be expected for various prospective applications.

One important approach to generate mesoporous materials of various structures is to add certain organic additives in synthesis systems. There are many reports about the effect of the organic additives on the structures of mesoporous materials, especially on the phase evolution in the cases using PEO-PPO-PEO as the SDA in the aqueous-phase system [14,16–25]. It has been found that the addition of hydrophobic organic molecules such as alkanes and 1,3,5-trimethylbenzene (TMB) not only significantly expands the mesopore size due to the pore-swelling effect [14,16], but also tend to promote the formation of mesostructures with spherical mesopores, particularly at high addition amount [17–20]. Such an effect primarily results from the requirement to cover the introduced swelling agent with a limited amount of SDAs [19]. In contrast, the addition of small hydrotropic molecules such as *n*-butanol can dramatically reduce the curvature of the PEO-PPO-PEO micelles [21–24]. It is due to the fact that the alcohol molecules can interact with both the hydrophilic PEO and hydrophobic PPO blocks, thus reside at the hydrophilic–hydrophobic interface of the micelle, thus co-micellizing with the block copolymer [23,24]. Considering the findings mentioned above, we suppose that such two contrasting effects may converge if the PPO homopolymer is utilized as the additive, because PPO homopolymer has the same composition as the PPO segment of the amphiphilic template and represents an additive with medium hydrophilicity located between the conventional hydrophobic swelling agent and the hydrotropic alcohols. To date, no work has been done to systematically investigate the phase evolution effect induced by the addition of PPO homopolymer, despite that its slight pore-swelling effect was reported [25,26].

Evaporation induced self-assembly (EISA) method has been frequently adopted for the synthesis of ordered mesoporous materials because of its applicability for a wide range of SDAs [7,8,27–29]. However, when conventional additives such as alkanes, TMB and *n*-butanol, are introduced in the EISA approach, the self-assembly between the SDAs and the precursors would be influenced. Due

* Corresponding authors. Tel.: +86 21 5566 4194; Fax: +86 21 5566 4192.
E-mail addresses: yhdeng@fudan.edu.cn (Y. Deng), dyzhao@fudan.edu.cn (D. Zhao).

1387-1811/$ - see front matter © 2008 Elsevier Inc. All rights reserved.
doi:10.1016/j.micromeso.2008.05.043

to the weak interactions between the additive and hydrophobic PPO block in the non-aqueous polar solutions used in EISA process, the additive may not fully participate in the self-assembly of the composite micelle, which caused the inhomogeneous distribution of the additives within the synthesis system, leading to disordered mesostructures or even macrophase separation [26,30]. As a result, few papers have been reported to study the phase evolution effect of organic additives in EISA approach [30]. Naik et al. [30] found the rod-to-sphere transition with hydrophobic 1,3,5-triisopropylbenzene (TIPB) as the additive and cetyltrimethylammonium bromide (CTAB) as the templates through EISA method. However, due to the strong hydrophobicity of TIPB, numerous TIPB oil droplets were observed, suggesting that a macrophase separation occurred. Therefore, it is difficult to investigate quantitatively and systematically the phase evolution induced by TIPB. To date, except for those with mixed surfactants [31], no work has been done to study the phase evolution of non-surfactant additive on the synthesized mesostructures using PEO-PPO-PEO as the SDA in EISA method.

In this paper, we aim to investigate the phase evolution of mesoporous silica in the EISA approach by using low molecular weight homopolymer poly(propylene oxide) (M_n = 400) (PPO400) as the additive. It is found that the addition of PPO400 can cause hydrotropic curvature-reducing effect on the mesostructures. Upon the increase of PPO400 amount, the structures of the obtained mesoporous silicas gradually evolve from three-dimensional (3-D) cubic $Im\bar{3}m$ to quasi-*p6m*, to hexagonal *p6m*, and to mixed structures consisting of lamellar and reversed cylindrical structure. The quasi-*p6m* mesoporous silica structure has the buckled cylindrical mesopores [19,32] with intermediate curvature and acts as the metastable structure during the phase evolution from $Im\bar{3}m$ to *p6m* structure, in accordance with the epitaxial relationship [33]. This curvature-reducing effect is mainly attributed to the relatively weak hydrophobicity and good compatibility of PPO400 homopolymer.

2. Experimental

2.1. Chemicals

Triblock poly(ethylene oxide)-*b*-poly(propylene oxide)-*b*-poly(ethylene oxide) copolymer Pluronic F127 ($EO_{106}PO_{70}EO_{106}$, M_n = 12600) was purchased from Aldrich. Poly(propylene oxide) homopolymer (M_n = 400, PPO400), and poly(propylene oxide) homopolymer (M_n = 4000, PPO4000) were purchased from Alfa-Aesar. Tetraethyl orthosilicate (TEOS) and ethanol were purchased from Shanghai Chemical Company. All chemicals were used as received without any further purification. Millipore water was used in this study.

2.2. Sample preparation

The synthesis of mesoporous silicas were carried out through EISA process similar to that for SBA-16 [28], except that PPO homopolymer was added. In the case that PPO400 was the additive, a series of samples were prepared according to the following procedure. About 1.0 g of F127 and 0.1–1.20 g of PPO400 were first dissolved in 15.0 g of ethanol, then 0.90 g of H_2O, 0.10 g of 2 M HCl aqueous solution, and 2.08 g of TEOS were added under magnetic stirring. After stirring for 1 h, the obtained homogeneous solution was poured into Petri dishes to allow solvent evaporation for 24 h at room temperature. The as-made films were collected and calcined in air at 550 °C for 5 h, with heating rate of 1 °C/min. The obtained samples were designated as Si-PPO400-*X*, where *X* refers to the weight percent of PPO400 relative to F127. In the case with PPO4000 as the additive, the synthesis was carried out through the same procedure as that for Si-PPO400-*X*, and the obtained samples were designated as Si-PPO4000-*Y*, wherein *Y* refers to the weight percent of PPO4000 relative to F127.

2.3. Characterization

The small-angle X-ray diffraction (XRD) was performed on a German Bruker D4 X-ray diffractometer with Ni-filtered Cu Kα radiation. The transition electron microscopy (TEM) images were obtained with a JEOL 2011 microscope operated at 200 kV. Before TEM measurement, the powder samples were dispersed in ethanol, and then dipped and dried on Cu grids. Nitrogen adsorption–desorption isotherms were measured at 77 K by using a Micromeritics ASAP Tristar 3000 system. The samples were degassed at 180 °C overnight on a vacuum line. The Brumauer-Emmett-Teller (BET) method was utilized to calculate the specific surface areas. The pore size distributions of the calcined samples were derived from the adsorption branches of the isotherms based on BJH method (for cylindrical mesopores), and Broekoff-de Boer (BdB) sphere model (for spherical mesopores).

3. Results and discussion

In this study, we fixed the amount of F127, TEOS, H_2O, HCl and ethanol, then varied the amount of homopolymer PPO to study the phase evolution of the obtained final structure of mesoporous silica. All the data of our samples are summarized in Table 1. With PPO400 as the additive, all the as-made composite films obtained after solvent evaporation are homogeneous in appearance, suggesting a good compatibility of the PPO400 in the composites. Small-angle XRD patterns of the calcined Si-PPO400-X at 550 °C are displayed in Fig. 1. Si-PPO400-0 obtained without addition of PPO400 shows four well-resolved diffraction peaks at 2θ values of 0.83, 1.14, 1.38 and 2.10°, assigned to the 1 1 0, 2 0 0, 2 1 1, and 2 2 2 reflections of highly ordered cubic mesostructure with space group of $Im\bar{3}m$ (Fig. 1a). Interestingly, when adding PPO400 to 10 wt%, the obtained Si-PPO400-10 sample shows a different well-resolved XRD patterns (Fig. 1b). Three diffraction peaks at 2θ values of 0.90, 1.80, and 2.37° can be observed, which can be indexed to the 1 0, 2 0 and 2 1 reflections of highly ordered *p6m* mesostructure (Fig. 1b). The 2-D hexagonal mesostructure can be preserved even when the PPO400 addition is increased to 90 wt%, indicating a wide synthesis range (Fig. 1c–g). The lattice constant of these mesostructures are calculated to be about 11 nm, as shown in Table 1. No significant increase in the cell parameter of the obtained *p6m* mesostructure was detected, suggesting that the pore-swelling ability of the low molecular weight homopolymer PPO400 is negligible (Table 1). It is worth noting that, resolved XRD patterns with 1 0, 1 1, and 2 0 diffraction peaks can be clearly observed for the samples obtained with higher PPO400 addition amount (70–90 wt%) (Fig. 1f and g). By contrast, in the cases of samples obtained with lower PPO400 amount (40–60 wt%), no 1 1 diffraction peak was detected, but a new diffraction peak assigned to the 2 1 diffraction appeared instead. This difference in the diffraction intensities can be attributed to the uniaxial lattice distortion during the solvent evaporation [7,8,32,34]. Notably, the 1 1 diffraction peak was detected for the samples with more PPO400 added (Fig. 1f and g). It may suggest that PPO400 can relieve lattice distortion, probably since the nonvolatile liquid PPO400 could prevent the as-synthesized film from the contraction caused by the complete evaporation of solvent. When the addition amount of PPO400 is comparable to that of F127 (i.e. 100 and 120 wt%), the obtained samples (Si-PPO400-100 and Si-PPO400-120) display only two weak XRD diffraction peaks at 2θ of about 1.3 and 2.7°, with *d*-spacing ratio of 1:2, implying the possible formation of lamellar structure (Fig. 1h and i).

Table 1
The textural properties of the mesoporous silica products obtained by using PPO homopolymer as the additive from EISA approach at room temperature

Sample name	Structure	*d*-spacing (nm)[a]	Unit cell parameter *a*[b] (nm)	Pore size *D* (nm)	Wall thickness *H*[e] (nm)	BET surface area[f] (m^2/g)	Pore volume (cm^3/g)
Si-PPO400-0	$Im\bar{3}m$	10.6	15.0	10.6[c]	3.8	238.8	0.30
Si-PPO400-10	quasi-*p6m*	9.78	11.3	7.9[c]/5.8[d]	3.4[c]/5.5[d]	243.5	0.35
Si-PPO400-20	*p6m*	9.7	11.2	6.6[d]	4.6	243.3	0.39
Si-PPO400-30	*p6m*	9.87	11.4	6.7[d]	4.7	239.7	0.41
Si-PPO400-40	*p6m*	9.53	11.0	6.6[d]	4.4	247.7	0.28
Si-PPO400-50	*p6m*	9.87	11.4	6.4[d]	5.0	234.1	0.25
Si-PPO400-60	*p6m*	9.20	10.6	5.4[d]	5.2	223.4	0.28
Si-PPO400-70	*p6m*	10.2	11.8	7.1[d]	4.7	274.4	0.35
Si-PPO400-80	*p6m*	8.92	10.3	6.9[d]	3.4	239.9	0.30
Si-PPO400-90	*p6m*	10.4	12.0	7.0[d]	5.0	239.8	0.31
Si-PPO400-100	Mixed	6.5	6.5	–	–	37.2	0.07
Si-PPO400-120	Mixed	6.7	6.7	–	–	30.2	0.05
Si-PPO4000-30	Disordered			11.1[c]	–	129.2	0.15
Si-PPO4000-60	Disordered			11.7[c]	–	148.1	0.23
Si-PPO4000-90	Disordered			11.6[c]	–	200.3	0.30

[a] Calculated from XRD results. For mixed phase, the *d*-spacing is defined as 10 reflection of a lamellar structure; for cubic $Im\bar{3}m$ structure, the *d*-spacing is calculated from the (110) reflection, for 2-D hexagonal p6m structure, the *d*-spacing is calculated from the 10 reflection.
[b] For hexagonal *p6m* structure, $a = 2d_{10}\sqrt{3}$, and for cubic $Im\bar{3}m$, $a = d_{110}\sqrt{2}$.
[c] Calculated by the BdB model from the adsorption branches of the isotherms.
[d] Calculated by the BJH model form the adsorption branches of the isotherms.
[e] Calculated from the formulas $h = \sqrt{3}(a - D)/2$, $h = a - D$, for cubic $Im\bar{3}m$, and hexagonal *p6m* mesostructure respectively, where *a* represents the unit cell parameter and *D* represents the pore diameter determined by N_2 sorption isotherms. The wall thickness of Si-PPO-10 was calculated according to the hexagonal mesostructure.
[f] Calculated by the BET model from sorption data in a relative pressure range from 0.04 to 0.2.

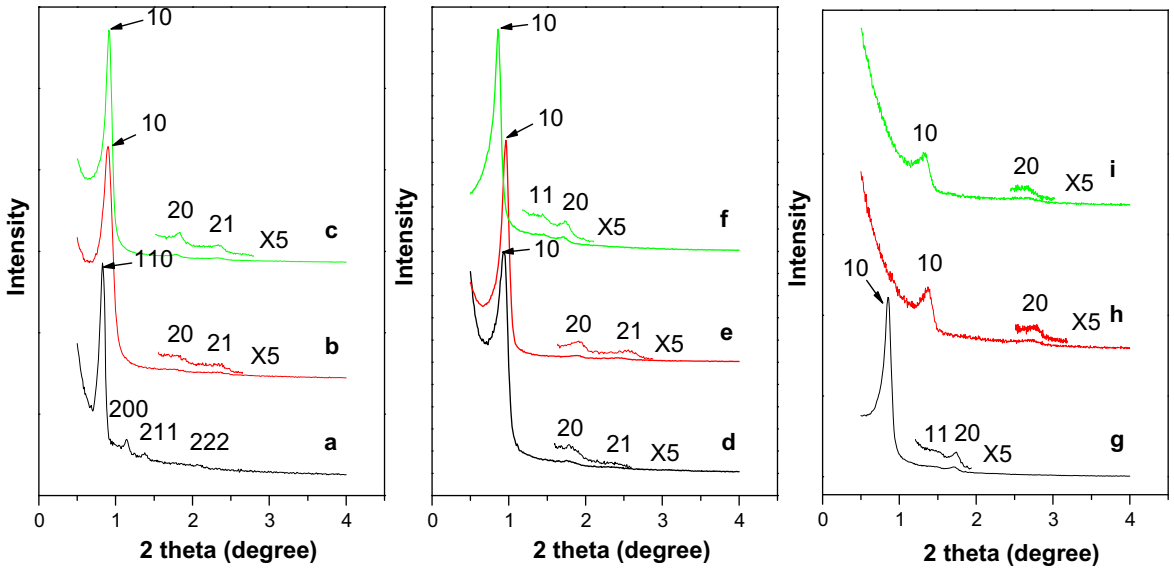

Fig. 1. Small-angle XRD patterns of mesoporous silicas calcined at 550 °C with different addition amount of PPO400 homopolymer: (a) 0%, Si-PPO400-0; (b) 10%, Si-PPO400-10; (c) 20%, Si-PPO400-20; (d) 40%, Si-PPO400-40; (e) 60%, Si-PPO400-60; (f) 70%, Si-PPO400-70; (g) 90%, Si-PPO400-90; (h) 100%, Si-PPO400-100; and (i) 120%, Si-PPO400-120.

TEM images were taken to further investigate the mesostructures of the obtained samples with different addition amount of PPO400. Without PPO400, the Si-PPO400-0 sample shows typical TEM images of body-centered cubic mesostructure viewed along the [100], [110], and [111] directions, similar with that of SBA-16, confirming a highly ordered mesostructure. The sample Si-PPO-400-10 with 10 wt% PPO400 shows high degree of periodicity over large domains, viewed from different directions (Fig. 2a–c). Interestingly, although the small-angle XRD data indicate mesostructure of *p6m* symmetry, the cylindrical mesopores are found to be a buckled cylindrical structure [19] with spherical-like mesopores within the channels in domains of the same mass contrast, which is very different from the conventional cylindrical mesopores of *p6m* structure such as that of SBA-15. Some regions with mixed phases of the normal hexagonal *p6m* structure and the buckled cylindrical structure are observed (Fig. 2c). TEM image with larger magnification (Fig. 2d) further reveals that the spherical mesopores are within the channels even at the edge of the sample, excluding the possibility of orthogonal overlapping of two domains. These results suggest that sample S-PPO400-10 has a quasi-*p6m* buckled cylindrical mesostructure with curvature intermediate between cubic $Im\bar{3}m$ and hexagonal *p6m* structure [19]. Such a buckled cylindrical structure is the intermediate captured during the phase transformation from the $Im\bar{3}m$ to *p6m* structure [32,33]. Lettow et al. [19] also observed similar buckled cylindrical mesopore structure during the structure evolution from SBA-15 with *p6m* symmetry to mesostructured cellular foams (MCF) in the aqueous synthesis approach using Pluronic P123 as a template

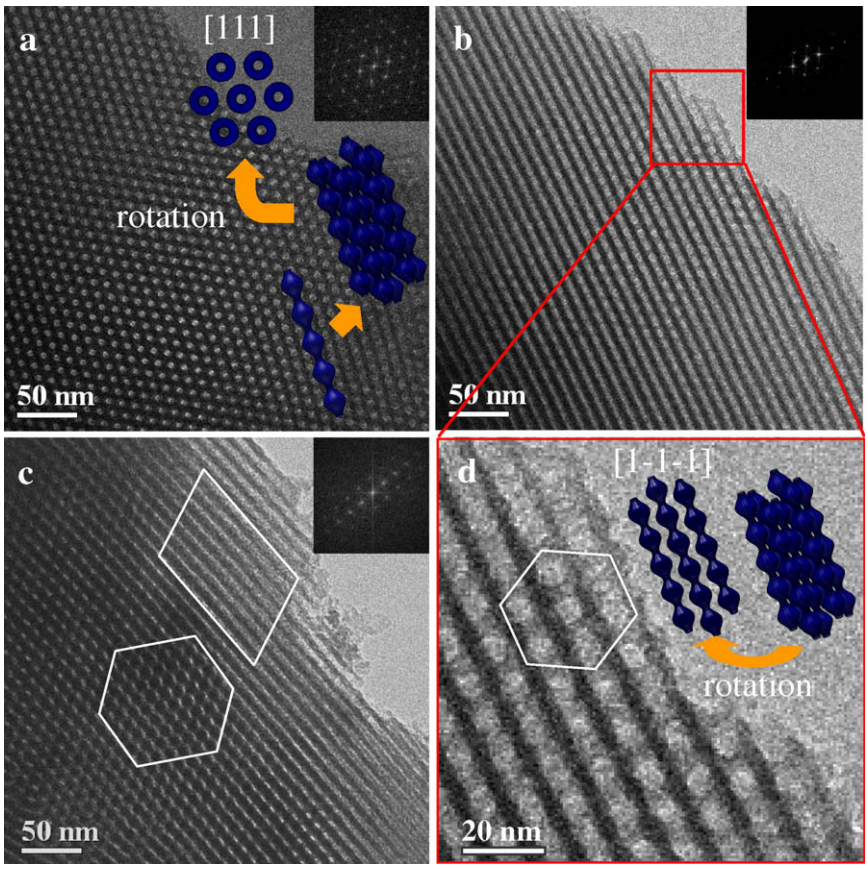

Fig. 2. TEM images of Si-PPO400-10 with quasi-*p6m* symmetry, showing: (a) typical hexagonal mesopore structure, (b) buckled cylindrical mesostructure, (c) mixed phases with transition region between the buckled cylindrical structure and the normal hexagonal *p6m* structure, and (d) the magnified image of part b. The insets are the corresponding Fourier transform (FFT) diffractograms. The models inset in the part a and part d are the isosurfaces of the mesopores with quasi-*p6m* buckled cylindrical structure viewed along the [1 1 1] (a) and the [1-1-1] axes (d) of the original $Im\bar{3}m$ structure. Compression along the [1 1 1] axis of the $Im\bar{3}m$ structure may occurs during the phase transformation, therefore the angle between [1 1 1] and [1-1-1] axes is smaller than 109°28′ and closer to 90°.

and TMB as an additive. Further increasing the amount of PPO400 to 20 wt% and even to 70 wt%, the typical cylindrical mesopore arrays with ordered hexagonal *p6m* symmetry for Si-PPO400-20 and Si-PPO400-70 samples can be observed in their respective TEM images (Fig. 3). No buckled cylindrical mesopores are found, implying that the phase evolution from $Im\bar{3}m$ to *p6m* symmetry is accomplished. The cell parameters for both samples estimated from the TEM images are around 11.0 nm, in good agreement with that from XRD patterns. When the PPO400 amount increases to 100 wt%, a lamellar mesostructure for Si-PPO400-100 sample is observed in the TEM images (Fig. 4a and b), well agreeing with the XRD patterns (Fig. 1i). The lattice constant is measured to be 6.1 nm from the magnified TEM images (Fig. 4b), close to the value (6.5 nm) calculated from the XRD diffraction (Table 1). Additionally, silica nanowires are also observed in some domains under TEM observations (Fig. 4c and d). The diameter of the nanowires is about 8 nm, slightly larger than the *d*-spacing of lamellar mesostructure. These results suggest the coexistence of the reversed cylindrical micelles in some microdomains during EISA process with 100 wt% PPO400 addition. In these microdomains, the PPO400 homopolymer behaves as oily continuous phase. Previous studies show that, in the EISA process, the formation of reversed cylindrical micelles and therefore silica nanowires occurs only when nonpolar and strongly hydrophobic solvents such as toluene and xylene are utilized as additives [35,36]. The strong hydrophobicity of the solvent is the predominant factor in those cases. Our observations indicate that the reversed cylindrical structure could also be formed in less hydrophobic solvent such as homopolymer PPO400. However, the coexistence of the lamellar phase implies that PPO400 homopolymer is not hydrophobic enough to induce complete formation of reversed cylindrical structure to generate pure silica nanowires as reported in the Ref. [35–37].

Nitrogen adsorption–desorption isotherms of calcined Si-PPO400-0 without adding PPO400 exhibits typical type-IV curves with a large H2-type hysteresis loop (Fig. 5Aa and Ba), suggesting a caged mesostructure. A sharp capillary condensation in the relative pressure (P/P_0) between 0.7 and 0.8 is observed, indicating a narrow pore size distribution centered at 10.6 nm (Fig. 5a). The sample Si-PPO400-10 shows similar type-IV isotherms with H2-type hysteresis loop, but the sharp capillary condensation occurred at a lower relative pressure (P/P_0) ranging from 0.6 to 0.7, implying a smaller mesopore size. The mean mesopore size is calculated to be about 5.6 nm from the adsorption branch (Fig. 5Ab and Bb). Its H2-type hysteresis loop further confirms with its quasi-*p6m* buckled cylindrical mesostructure, which has small pore window size similar with that for the $Im\bar{3}m$ mesostructure. Typical type-IV isotherms with H1-type hysteresis loop are observed for Si-PO400-40 (Fig. 5Ac), suggesting a cylindrical mesochannel. Isotherms with curves similar to those of Si-PPO400-40 are detected for the samples with larger amount of PPO400 (Si-PPO400-70 and Si-PPO400-90), further confirming that 2D hexagonal *p6m* mesostructure is formed with increased amount of PPO400 (Fig. 5Ad and Ae). The pore size distributions derived from the adsorption branches is not increased significantly upon the increase of PPO400 amount (Table 1). It is noteworthy that, compared to other samples with *p6m* symmetry, although Si-PPO400-10 has a much smaller window size which is not typical for a hexagonal *p6m* structure, it has similar pore size with the

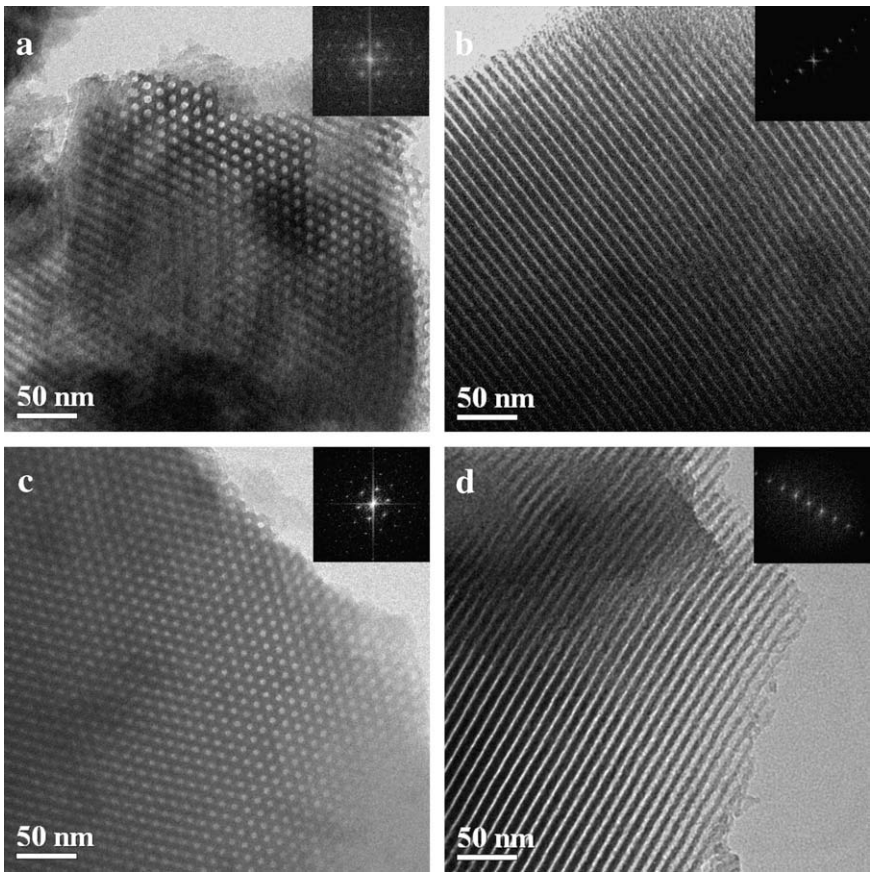

Fig. 3. TEM images of calcined Si-PPO400-20 (a, b) and Si-PPO400-70 (c, d) viewed from [1 0] and [0 1] directions of hexagonal *p6m* mesostructure, respectively; the insets are the corresponding FFT diffractograms.

samples having *p6m* structure when more PPO400 is added (Fig. 5B). It further corroborates previous presumption, indicating that Si-PPO400-10 is an intermediate structure different from that of its neighbouring samples during a gradual phase evolution from $Im\bar{3}m$ to *p6m* structure.

On the basis of the above results, we speculate that the phase evolution from $Im\bar{3}m$ to *p6m* mesostructure is related to the epitaxial relationship between the two phases [33,38], although further investigation is required to fully exclude the possibility of other structures such as $Fm\ \bar{3}\ m$. In accordance with the epitaxial relationship [33], the *d*-spacing of the (1 1 0) plane for $Im\bar{3}m$ mesostructure (10.6 nm for sample Si-PPO400-0) is close to that of the (1 0) plane in *p6m* structure (Fig. 1, Table 1), suggesting that no significant volume change of the lattice occurs. Moreover, the phase evolution is realized by the elongation of spherical mesopores or compression of the lattice along the [1 1 1] axis of the $Im\bar{3}m$ structure, therefore interconnecting mesopores and reducing the curvature of the mesopore simultaneously. The observed quasi-*p6m* buckled cylindrical mesostructure is an intermediate phase during this evolution, and the TEM observations can be explained by our simulated model of the buckled cylindrical structure derived from the epitaxial relationship (Fig. 2). The model of the buckled cylindrical structure indicates that the TEM images viewed along the [10] direction [1 1 1] direction in the original $Im\bar{3}m$ structure) is the same as the typical hexagonal *p6m* mesostructure, but images viewed along the [0 1] direction ([1-1-1] direction in the original $Im\bar{3}m$ structure) show spherical pores in a hexagonal pattern within the mesopore channels. This coincides well with our obtained TEM images. The reason to the existence of this epitaxial relationship during the phase evolution is possibly caused by lowering the kinetic barrier between the phases, which avoids the existence of metastable states of higher energies [38].

Based on above results, it is concluded that the homopolymer PPO400 behaves as the hydrotropic additive which can reduce the curvature of mesostructures and induce the phase transformation from spherical $Im\bar{3}m$ structure (with positive curvature) to finally the mixed phase of lamellar (with zero curvature) and reversed cylindrical structures (with negative curvature) (Scheme 1). Two main factors may contribute to its hydrotropic behavior. One is the relatively weak hydrophobicity of PPO with low molecular weight, which leads to weak-segregation [39,40], much different from those strongly hydrophobic molecules such as TMB with strong-segregation [41]. Therefore, it does not require the increase of curvature to cover the increasing additive with a fixed amount of surfactants [19]. Another is the good compatibility of PPO400 homopolymer with hydrophobic PPO block, which results that the former tends to distribute more uniformly within the composite micelles and thus increases the entropy of mixing, rather than merely at the hydrophobic cores of the composite micelles. This entropy effect requires the micelles to provide room for the PPO400 located at the outer corona or at the hydrophobic–hydrophilic interface [42], which makes the PPO400 serve as hydrotropic molecules, resulting in curvature reduction. Both of the factors help PPO400 to reside at the hydrophilic–hydrophobic interface of the micelle and participate in the micellization of the template (F127) molecules just like hydrotropic alcohols [21–24]. Other factors such as its nonvolatility and its miscibility with ethanol also favor the process of the phase evolution. The former makes it possible to investigate quantitatively, and the latter avoids the possible

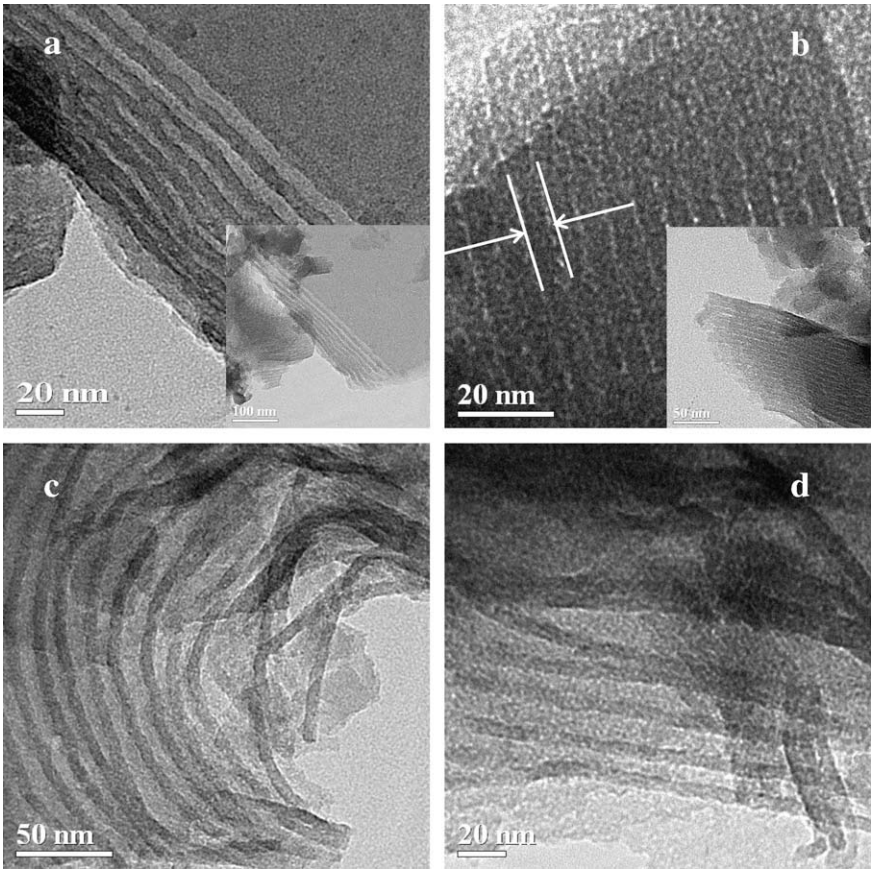

Fig. 4. TEM images of the sample Si-PPO400-100 showing (a, b) lamellar mesostructure viewed from different directions, and (c, d) the silica nanowires of ~8 nm. The insets are images of lower magnification.

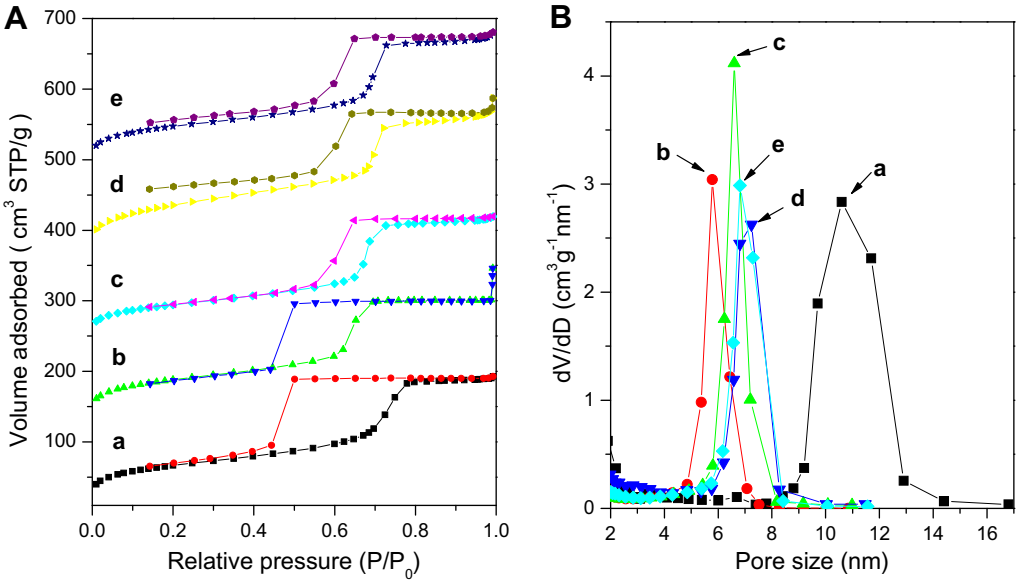

Fig. 5. Nitrogen adsorption–desorption isotherms (A) and the pore size distribution (B) of the calcined mesoporous silicas prepared with different addition amount of PPO400. (a) Si-PPO400-0; (b) Si-PPO400-10; (c) Si-PPO400-40; (d) Si-PPO400-70; and (e) Si-PPO400-90. The isotherms of (b)–(e) in the Figure A are offset vertically by 120, 240, 360, 480 cm^3/g, consecutively.

macrophase separation that leads to formation of oil droplets. We also found that the addition of PPO in the conventional aqueous synthesis has no effect on the product due to the good compatibility of PPO with water, and this result is consistent with the report by Park et al. [25].

When larger homopolymer PPO4000 was utilized as the additive, uneven composite films with visible oil droplet were obtained, clearly indicating that a macrophase separation occurs. Only one broad diffraction peak is observed from the small-angle XRD patterns of the calcined samples with PPO4000 addition of 30–

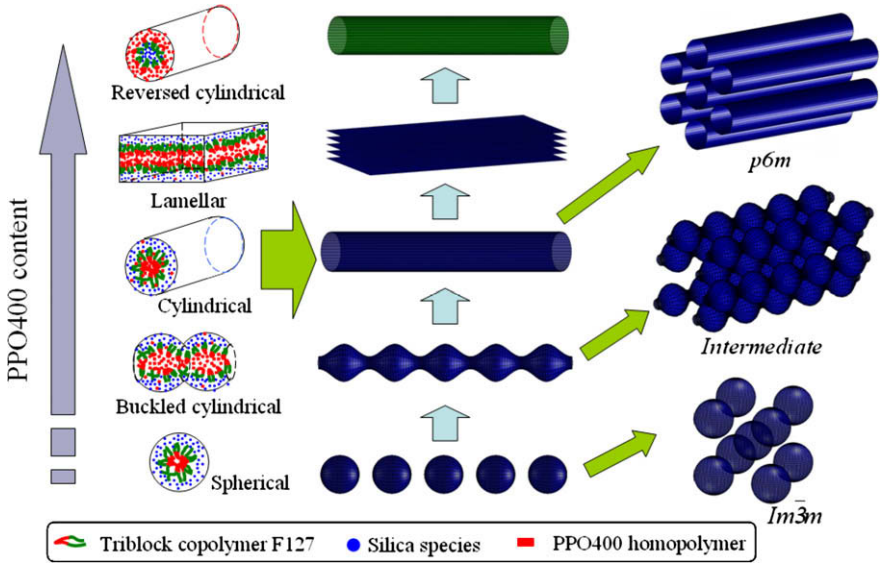

Scheme 1. Schematic illustration of the curvature-reducing effect of PPO400 homopolymer on the synthesized silica material via EISA method.

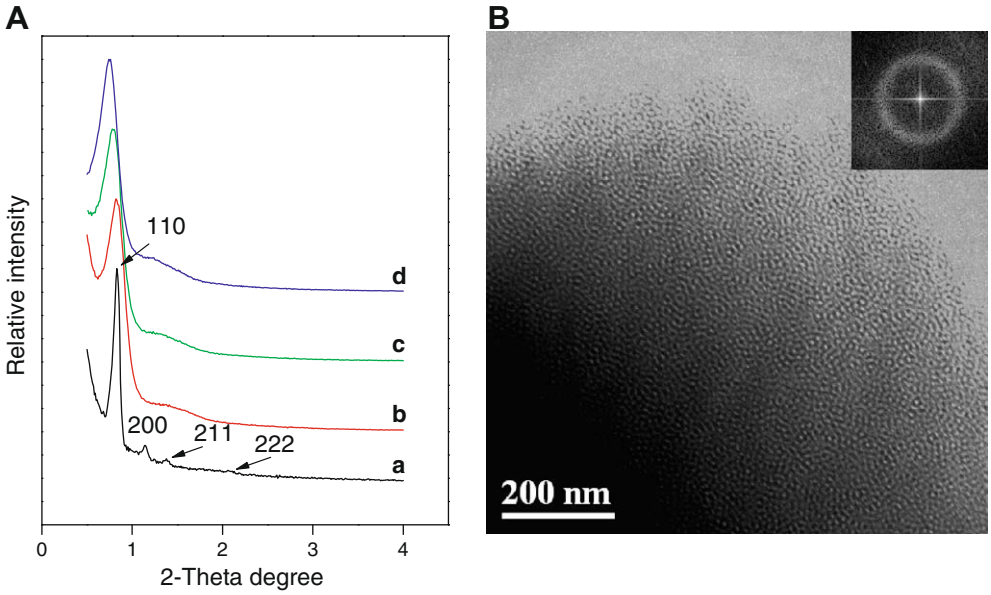

Fig. 6. Left: XRD pattern evolution of the calcined samples prepared with adding different amount of PPO4000 homopolymer. (a) Si-PPO4000-0; (b) Si-PPO4000-30; (c) Si-PPO4000-60; and (d), Si-PPO4000-90. Right: Representative TEM image of the calcined sample Si-PPO4000-30, showing the worm-like mesostructure.

90 wt% (Fig. 6, left), indicative of disordered mesostructure. The TEM image (Fig. 6, right) shows that Si-PPO4000-30 sample has worm-like mesopores. These results indicate that PPO4000 homopolymer hinders the self-assembly between F127 and silica oligomers during the EISA process and leads to macrophase separation as a result of aggregation of PPO4000 themselves. The effect of PPO homopolymers with different molecular weight reveals the relatively weak interaction between SDA and PPO homopolymer therefore highlights the importance of kinetic factors such as the diffusion of PPO molecules. Because of the fast solvent evaporation speed and relatively weak interaction, it will be difficult for PPO homopolymer molecules with large size to diffuse and then accommodates in the composite micelles, which eventually results in macrophase separation. Another possible explanation is that the molecular weight of PPO homopolymer also affects the thermodynamic compatibility of PPO with SDA/silica composite, similar as those found in the phase behavior of block copolymer/homopolymer composite [40]. This differentiates our current work from the report by Wu et al. in which PPO was used as a cotemplate in the CTAB-directed synthesis of mesoporous silica through aerosol-assisted technique [43], because our EISA method has a much slower solvent evaporation speed which makes it possible to present a more near thermodynamic result.

4. Conclusions

In this paper, we show the effects on the phase evolution induced by the addition of PPO homopolymer in the synthesis of mesoporous silica via EISA approach. PPO homopolymer with low-molecular weight (PPO400) can participate in the formation of composite micelles and greatly influence on the assembly of the mesostructure. A continuous mesostructure evolution from cu-

bic $Im\bar{3}m$ symmetry to quasi-*p6m*, to hexagonal *p6m*, finally to a mixed phase with lamellar and reversed cylindrical structure is observed. The quasi-*p6m* buckled cylindrical structure between the $Im\bar{3}m$ and *p6m* symmetry is successfully captured and proved to be an intermediate formed according to the epitaxial relationship during the phase evolution between these two phases. The homopolymer PPO400 behaves as a hydrotropic molecule and can reduce the curvature of the silica mesostructures with little pore-swelling effect, which is due to its relatively weak hydrophobicity and good compatibility with the PPO block of the template. With larger sized PPO4000 as the additive, only disordered mesostructure is observed, probably because of the poor diffusivity and compatibility which hinders the formation of composite micelles and only leads to macrophase separation.

Acknowledgments

This work was supported by the NSF of China (20721063, 20521140450 and 20641001), the State Key Basic Research Program of the PRC (2006CB932302) and Shanghai Sci. & Tech. Committee (06DJ14006 and 0652nm024), Shanghai Key Laboratory of Green Chemistry and Chemical Processes, East China Normal University, Shanghai 200062, China and Shanghai Leading Academic Discipline Project (B108).

References

[1] C.T. Kresge, M.E. Leonowicz, W.J. Roth, J.C. Vartuli, J.S. Beck, Nature 359 (1995) 1299–1303.
[2] J.S. Beck, J.C. Vartuli, W.J. Roth, M.E. Leonowica, C.T. Kresge, K.D. Schmitt, C.T.W. Chu, D.H. Olson, E.W. Sheppard, S.B. McCullen, J.B. Higgins, J.L. Schlenker, J. Am. Chem. Soc. 114 (1992) 10834–10843.
[3] A. Corma, Chem. Rev. 97 (1997) 2373–2419.
[4] J.A. Melero, R. van Grieken, G. Morals, Chem. Rev. 106 (2006) 3790–3812.
[5] J.B. Scott, G. Wirnsberger, G.D. Stucky, Chem. Mater. 13 (2001) 3140–3150.
[6] I.I. Slowing, B.G. Trewyn, S. Giri, V.S.-Y. Lin, Adv. Func. Mater. 17 (2007) 1225–1236.
[7] Y. Wan, Y.F. Shi, D.Y. Zhao, Chem. Commun. (2007) 897–926.
[8] Y. Wan, D.Y. Zhao, Chem. Rev. 107 (2007) 2821–2860.
[9] Y. Wan, H.F. Yang, D.Y. Zhao, Acc. Chem. Res. 39 (2006) 423–432.
[10] P.T. Tanev, T.J. Pinnavaia, Science 267 (1995) 865–867.
[11] S.A. Bagshaw, E. Prouzet, T.J. Pinnavaia, Science 269 (1995) 1242–1244.
[12] G.S. Attard, J.C. Glyde, C.G. Glotner, Nature 378 (1995) 366–367.
[13] M. Templin, A. Franck, A. Duchesne, H. Leist, Y.M. Zhang, R. Ulrich, V. Schadler, U. Wiesner, Science 278 (1997) 1795–1798.
[14] D.Y. Zhao, J.L. Feng, Q.S. Huo, N. Melosh, G.H. Fredrickson, B.F. Chmelka, G.D. Stucky, Science 279 (1998) 548–552.
[15] D.Y. Zhao, Q.S. Huo, J.L. Feng, B.F. Chmelka, G.D. Stucky, J. Am. Chem. Soc. 120 (1998) 6012–6036.
[16] J. Fan, C.Z. Yu, L.M. Wang, B. Tu, D.Y. Zhao, Y. Sakamote, O. Terasaki, J. Am. Chem. Soc. 123 (2001) 12113–12114.
[17] P. Schmidt-Winkel, W.W. Lukens Jr., D.Y. Zhao, P.D. Yang, B.F. Chmelka, G.D. Stucky, J. Am. Chem. Soc. 121 (1999) 254–255.
[18] P. Schmidt-Winkel, W.W. Lukens Jr., P.D. Yang, D.I. Margolese, J.S. Lettow, J.Y. Ying, G.D. Stucky, Chem. Mater. 12 (2000) 686–696.
[19] J.S. Lettow, Y.J. Han, P. Schmidt-Winkel, P.D. Yang, D.Y. Zhao, G.D. Stucky, J.Y. Ying, Langmuir 16 (2000) 8291–8295.
[20] M. Luechinger, G.D. Pirngruber, B. Lindlar, P. Laggner, R. Prins, Micropor. Mesopor. Mater. 79 (2005) 41–52.
[21] F. Kleitz, S.H. Choi, R. Ryoo, Chem. Commun. (2003) 2136–2137.
[22] F. Kleitz, L.A. Solovyov, G.M. Anilkumar, S.H. Choi, R. Ryoo, Chem. Commun. (2004) 1536–1537.
[23] T.-W. Kim, F. Kleitz, B. Paul, R. Ryoo, J. Am. Chem. Soc. 127 (2005) 7601–7610.
[24] P.Y. Feng, X.H. Bu, D.J. Pine, Langmuir 16 (2000) 5304–5310.
[25] B.-G. Park, W. Guo, X. Cui, J. Park, C.-S. Ha, Micropor. Mesopor. Mater. 66 (2003) 229–238.
[26] Y.K. Hwang, K.R. Patil, S.H. Jhung, J.-S. Chang, Y.J. Ko, S.-E. Park, Micropor. Mesopor. Mater. 78 (2005) 245–253.
[27] Y.F. Lu, R. Ganguli, C.A. Drewien, M.T. Anderson, C.J. Brinker, W.L. Gong, Y.X. Guo, H. Soyez, B. Dunn, M.H. Huang, J.I. Zink, Nature 389 (1997) 364–368.
[28] D.Y. Zhao, P.D. Yang, N. Melosh, J.L. Feng, B.F. Chmelka, G.D. Stucky, Adv. Mater. 10 (1998) 1380–1385.
[29] B.Z. Tian, X.Y. Liu, Z.D. Zhang, B. Tu, D.Y. Zhao, J. Solid State Chem. 16 (2000) 324–329.
[30] S.P. Naik, W. Fan, T. Yokoi, T. Okubo, Langmuir 22 (2006) 6391–6397.
[31] Y. Huang, H.Q. Cai, T. Yu, X.L. Sun, B. Tu, D.Y. Zhao, Chem. Asian J. 2 (2007) 1282–1289.
[32] E.L. Crepaldi, G.J. de A.A. Soler-Illia, D. Grosso, F. Cagnol, F. Ribot, C. Sanchez, J. Am. Chem. Soc. 125 (2003) 9770–9786.
[33] P. Sakya, J.M. Seddon, R.H. Templer, R.J. Mirkin, G.J.T. Tiddy, Langmuir 13 (1997) 3706–3714.
[34] D. Grosso, F. Cagnol, G.J. de A.A. Soler-Illia, E.L. Crepaldi, H. Amenitsch, A. Brunet-Bruneau, A. Bourgeois, C. Sanchez, Adv. Func. Mater. 14 (2004) 309–322.
[35] C.Z. Yu, B.Z. Tian, J. Fan, B. Tu, D.Y. Zhao, Chem. J. Chin. Univ. 24 (2003) 5–8.
[36] C.Z. Yu, B.Z. Tian, J. Fan, G.D. Stucky, D.Y. Zhao, Chem. Lett. 31 (2002) 62–63.
[37] K. Yu, A.J. Hurd, A. Eisenberg, C.J. Brinker, Langmuir 17 (2001) 7961–7965.
[38] V. Luzzati, J. Phys. II 5 (1995) 1649–1653.
[39] M.W. Matsen, Macromolecules 28 (1995) 5765–5773.
[40] P.K. Janert, M. Schick, Macromolecules 31 (1998) 1109–1113.
[41] A.N. Semenov, Macromolecules 26 (1993) 2273–2281.
[42] H. Tanaka, H. Hasegawa, T. Hashimoto, Macromolecules 24 (1991) 240–251.
[43] Z.W. Wu, Q.Y. Hu, J.B. Pang, H.P. Jakobsen, D.H. Yu, Y.F. Lu, Micropor. Mesopor. Mater. 85 (2005) 305–312.